第 31卷第 12期　焊 接 学 报　Vol.31 No.12
2010年 12月　TRANSACTIONS OF THE CHINA WELDING INSTITUTION　December 2010

# X60管线钢在 −20 ℃低温焊接的接头组织性能

李建军[1,2]，杜则裕[1]，刘光云[2]，吕向阳[2]
（1. 天津大学 材料学院，天津 300072；2. 中国石油管道焊接培训中心，河北 廊坊 065000）

摘　要：结合 X60管线钢在 −20 ℃低温条件下的焊接施工实际情况进行了试验、测定及分析，研究了 ϕ711 mm×15.9 mm管道环焊接头的力学性能、接头的金相组织、硬度、冲击吸收功以及冲击断口形貌等．结果表明，在 −20 ℃低温条件下，焊接完成的 X60管线钢环焊接头力学性能测试；其 HAZ的最大硬度值为 210 HV10，符合相关技术标准．该工艺方案经过国内北部地区长输管道的工程使用，质量合格；经过金相显微组织分析，在 X60钢 −20 ℃条件下焊接的接头中，未发现淬硬组织；对冲击试件断口形貌的扫描电镜分析表明，该环焊接头的韧性满足相关技术标准的要求．

关键词：X60管线钢；−20 ℃低温焊接；焊接接头性能
中图分类号：TG457.6　文献标识码：A　文章编号：0253−360X（2010）12−0093−04


李建军

## 0 序　言

近年来，世界各国都非常重视石油天然气工业的建设与开发．国内国民经济的迅速发展，对于能源的需求量与日俱增．尤其最近十年，国内能源的结构状况在发生着重要的变化．采用管道输送石油天然气由于具有运输量大、经济性好、安全性高等许多优点，因此受到世界各国的重视[1]．当前管道建设的特点之一，就是油气田的资源大多为地质条件较差的沙漠、戈壁、人迹罕至的荒辟之地，或者是气温很低的寒带、永冻区，以及海洋的大陆架或深海地区等严酷环境，例如俄罗斯西伯利亚、英国北海油气田、北美阿拉斯加等地区．中国北部边境漠河、新疆等地都处于最低气温 −50～−60 ℃，甚至更低[2,3]．在这些地区修建油气管道及跨国长输管道，首先要解决的技术关键就是“低温下进行焊接”的研究课题．这是因为在低温条件下能够焊接出优质的焊接接头，就可以延长寒冷冬季的施工时间．否则，一年中可用于施工的天数很少，甚至无法进行大的工程项目施工．

关于在什么温度以上可以进行焊接施工，为了保证焊接质量，在什么温度以下，禁止焊接施工，国内的相关技术标准中，曾经明确规定过对于 5 ℃以下，当不采用技术措施时，不准许进行低合金钢的焊接施工．近年来的经济建设发展与技术进步，也使得相关行业都在思考及探讨低温条件下焊接的可能性．文中结合油气长输管道的焊接施工需要，进行了 X60管线钢管在 −20 ℃低温环境下的焊接工艺研究，并且对于该环焊接头的组织性能进行了测试及分析．

收稿日期：2010−05−31

## 1 试验方法

### 1.1 试验材料

试验材料为 X60管线钢管．其化学成分及力学性能见表 1及表 2．试验用的 X60管线钢管的直径为 711 mm，壁厚为 15.9 mm．试验用管材的规格与中国北部地区某管线工程的情况一致．

表 1　X60管线钢的化学成分（质量分数，%）
Table 1　Chemical composition of X60 pipeline steel

| C | Si | Mn | P | S | Nb | Ti | Fe |
|---|---|---|---|---|---|---|---|
| 0.14 | 0.41 | 1.44 | 0.016 | 0.09 | 0.05 | 0.02 | 余量 |

表 2　X60管线钢的力学性能
Table 2　Mechanical properties of X60 pipeline steel

| 抗拉强度 $R_m$/MPa | 屈服强度 $R_{eL}$/MPa | 冲击吸收功 $A_{KV(0℃)}$/J | 断后伸长率 A(%) |
|---|---|---|---|
| 545 | 415 | 149 | 33.0 |

X60钢属于“铁素体＋珠光体”类型的管线钢，与国家标准 GB/T 9711.2《石油天然气工业输送钢管》的 L415钢相当．X60钢母材的显微组织如图 1

所示. 从图 1中可以看到铁素体与珠光体的晶粒比较细小,组织均匀.

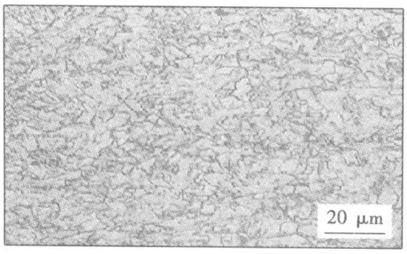

图 1 X60钢显微组织形貌
Fig. 1 Microscopic structure of X60 steel

1.2 施焊环境

施焊的环境温度为 −20 ℃;环境相对湿度为 70% RH;环境风速为 1 m/s. 将组装点固好的 X60钢管环焊接头置于上述低温环境中 4 h以上方可进行焊接试验. 焊前进行 100 ℃预热,焊后用石棉被覆盖缓冷.

1.3 焊接工艺

X60管线钢管的环焊缝焊接方案采用水平固定位置(5G位置)进行施焊. 根焊采用焊条电弧焊下向焊接,焊条型号为 AWS A5.1 E6010,直径为 3.2 mm;填充、盖面焊采用自保护药芯焊丝半自动焊,焊接方向为下向焊接,焊丝型号为 AWS A5.29 E71T8−Ni1,直径为 2.0 mm. 具体的焊接工艺参数如表 3所示.

表 3 X60管线钢管 5G位置焊接工艺参数
Table 3 Welding Parameters of X60 Pipeline Steel in 5G Position

| 焊道 | 焊接电流 I/A | 电弧电压 U/V | 焊接速度 $v/(\mathrm{cm\cdot min^{-1}})$ | 送丝速度 $v_s/(\mathrm{m\cdot min^{-1}})$ |
|---|---|---|---|---|
| 根焊 | 60~70 | 28~34 | 8~10 | — |
| 填充焊 | 190~240 | 17~18 | 13~18 | 2.0 |
| 盖面焊 | 180~230 | 17~18 | 9~10 | 2.0 |

1.4 焊后检测

环缝焊接完成后进行焊缝外观检测,其检测结果为合格. 然后,对该环焊接头进行 X射线检测,检测结果为合格. 质量检测的执行标准为中国石油行业标准 SY/T4103—2006《钢质管道焊接及验收》及瑞典标准 DNV—OS—F101《海洋管道系统》.

1.5 环焊接头的力学性能试验

根据中国石油行业标准 SY/T 4103—2006在 WAW—1000D型拉伸试验机上进行环焊接头力学性能测试,测定该环焊接头的抗拉强度 $R_m$. 并且进行刻槽锤断试验、面弯试验、背弯试验,以及在 JBN500型冲击试验机上进行环焊接头焊缝、熔合区及 HAZ的 V形缺口冲击吸收功的测定.

1.6 金相观察及维氏硬度测定

按照相关技术标准的规定,从该环焊接头截取金相试件,对于焊缝、熔合区及 HAZ部位进行金相显微组织观察. 使用的设备为 CMM—20E型金相显微镜. 在 432SVD型维氏硬度计上测定该接头的硬度分布及 $\mathrm{HV_{max}}$值.

1.7 冲击试样的断口分析

对于该环焊接头的冲击试样断口,使用 XL—30TMPE型扫描电镜进行断口分析.

## 2 试验结果及分析

2.1 力学性能

X60管线钢的环焊接头力学性能试验结果如表 4所示. 从表 4可知 X60管线钢在 −20 ℃条件下施焊的环焊接头 $R_m$ = 547~557 MPa. 该拉伸试件的断裂位置均为母材. 面弯、背弯的试验结果表明未见超标缺陷. 总之,该环焊接头的力学性能检测结果符合中国石油行业标准 SY/T 4103—2006《钢质管道焊接及验收》的技术要求,结论为合格.

表 4 X60管线钢环焊接头力学性能
Table 4 Mechanical properties of X60 girth welded joints

| 试样编号 | 抗拉强度 $R_m$/MPa | 刻槽锤断试验 | 面弯试验 | 背弯试验 |
|---|---|---|---|---|
| 1 | 554 | 未见超标缺陷 | 未见超标缺陷 | 未见超标缺陷 |
| 2 | 557 | 未见超标缺陷 | 未见超标缺陷 | 未见超标缺陷 |
| 3 | 548 | 未见超标缺陷 | 未见超标缺陷 | 未见超标缺陷 |
| 4 | 547 | 未见超标缺陷 | 未见超标缺陷 | 未见超标缺陷 |
| 结论 | 合格 | 合格 | 合格 | 合格 |

2.2 接头的金相组织分析

X60管线钢 −20 ℃条件下施焊的接头金相组织形貌如图 2,图 3所示.

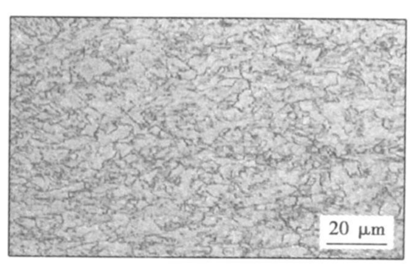

图 2 焊缝组织形貌
Fig. 2 Structure of weld

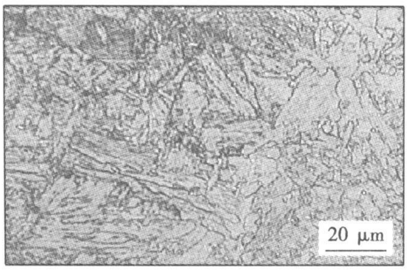

图 3　熔合区组织形貌
Fig.3　Structure of fusion zone

从图 2中可以看到焊缝中的柱状晶生长趋势.柱状晶的晶界是由先共析铁素体组成的,柱状晶内部是由块状先共析铁素体向晶内生长出来的细针及随后凝固结晶的珠光体组成的.在图 3中可以看到,焊缝的柱状晶是从受焊接热作用而出现的半熔化晶粒固液相界面开始生长的.其生长方向指向熔池中心,也就是与熔池中温度等于母材熔点的等温面垂直,并且与熔池散热方向相反.

在图 3中还可以观察到热影响区的粗大晶粒.同时,图 3与图 1进行比较也可以看出母材在焊接热输入的作用下,晶粒长大的情况是很严重的.显然,在 HAZ的粗晶区组织是脆化及硬化最为严重的区域.

## 2.3　接头的硬度分析

焊接接头的硬度测试数据如表 5所示,从表 5中可以看到该环焊接头的硬度分布情况.其中,第 7,11两个点的硬度数据分别为 206,210 HV10,这两个点就是在焊缝中心线两侧的硬度分布曲线的高峰,也就是焊接接头中的粗晶区硬度值.在该焊接接头中的最高硬度值为 210 HV10.该数据满足西气东输管道工程相关焊接及检测技术条件(XQ-CS-JX-SPE-0010)的有关规定.

## 2.4　冲击试验的数据及分析

X60钢 −20 ℃施焊的焊接接头冲击试验数据如表 6所示.冲击试验是根据中国石油行业标准

表 5　X60管线钢焊接接头硬度测试数据(HV10)
Table 5　Data of hardness test of X60 welded joints

| 测试点 | 1 | 2 | 3 | 4 | 5 | 6 | 7 | 8 |
|---|---|---|---|---|---|---|---|---|
| 硬度值 | 193 | 194 | 179 | 185 | 185 | 198 | 206 | 186 |
| 测试点 | 9 | 10 | 11 | 12 | 13 | 14 | 15 | 16 |
| 硬度值 | 194 | 185 | 210 | 185 | 183 | 183 | 185 | 185 |

SY/T 4103—2006《钢质管道焊接及验收》的技术要求在焊缝中心及熔合区部位开 V形缺口,进行冲击吸收功的测定.并且按照更为严格的瑞典标准 DNV-OS-F101《海洋管道系统》的技术要求,测定了离熔合区 2,5 mm(熔合区 +2 mm,熔合区 +5 mm)部位的冲击吸收功.

表 6　X60钢 −20 ℃施焊的环焊接头的冲击吸收功
Table 6　Impact absorbing energy of X60 girth welded joints at −20 ℃

| 缺口位置 | 冲击吸收功 $A_{KV(-20℃)}$/J | | | |
|---|---|---|---|---|
| | 实测值 | | | 平均值 |
| 焊缝 | 174 | 258 | 209 | 214 |
| 熔合区 | 315 | 310 | 296 | 307 |
| 熔合区 +2 mm | 328 | 314 | 328 | 323 |
| 熔合区 +5 mm | 325 | 330 | 333 | 329 |

从表 6中的数据可以看出,缺口位置依次在焊缝中心、熔合区、熔合区 +2 mm、熔合区 +5 mm时,冲击吸收功的平均值则由 214 J逐渐增大至 329 J,这就表明焊缝的冲击吸收功最低,熔合区的冲击吸收功增大了,直到“熔合区 +5 mm”处的冲击吸收功数值最高.该测试结果表明了在焊接接头内各区段的韧性变化规律.

## 2.5　冲击试样断口的电镜分析

−20 ℃低温条件下焊接的接头冲击试样扫描电镜断口形貌如图 4所示.从图 4a中可以看出,焊缝区的断口形貌呈片状的扇形花纹,是解理及准解理的断口.显然,这是由于焊缝属于铸造组织,其韧性比较低.熔合区的断口形貌如图 4b所示.熔合

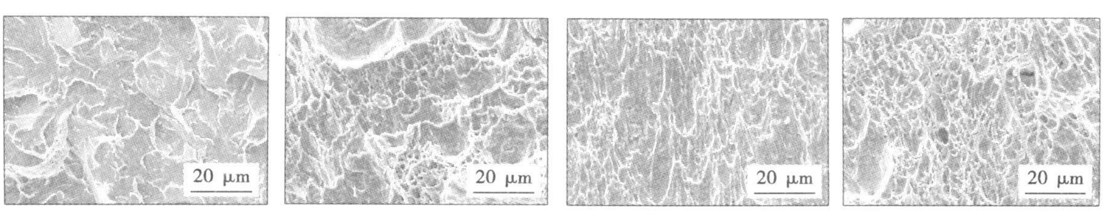


(a) 焊缝的断口形貌　(b) 熔合区的断口形貌　(c) “熔合区+2 mm”的断口形貌　(d) “熔合区+5 mm”的断口形貌

图 4　−20 ℃低温条件下焊接接头冲击试样扫描电镜断口形貌
Fig.4　SEM fracture structure of the joint impact sample cryo_weding at −20 ℃

区是焊缝与热影响区之间的交界处,这个地区的组织及成分的不均匀性比较突出. 因此,该区的断口则呈现出准解理的片状花纹与大韧窝状相结合的形貌. 图 4c,d分别是熔合区 +2 mm、熔合区 +5 mm 两个部位冲击试样的断口形貌. 比较这两个图可以看到,熔合区以外的焊接热影响区中的断口都属于韧性断裂的韧窝断口. 而且图 4d中韧窝状的形貌比较细小、均匀,优于图 4c中的形貌. 因此,图 4d 所显示的"熔合线 +5 mm"部位的韧性在上述的 4 个部位中是最好的. 这与冲击吸收功测试数据(表 6)所表明的规律性是一致的.

## 3 结 论

(1) X60管线钢环焊接头力学性能测试表明, $R_m$ = 547 ~557 MPa,拉伸试件断裂部位均在母材,接头力学性能测试的全部项目均达到合格;其 HAZ 的最大硬度值为 210 HV10,符合相关技术标准. 该工艺方案经过中国北部地区长输管道的工程使用,质量合格.

(2)经过金相显微组织分析,在 −20 ℃低温条件下焊接 X60钢环焊接头中,未发现淬硬组织.

(3)冲击试样断口形貌的电镜分析表明,该环焊接头的韧性满足中国石油行业标准 SY/T4103—2006《钢质管道焊接及验收》、瑞典标准 DNV—OS—F101《海洋管道系统》等相关技术标准的要求.

参考文献:

[1] 高惠临. 管线钢—组织 性能 焊接行为[M]. 西安: 陕西科学技术出版社, 1995.

[2] Cheaitani M. Advances in structural integrity assessment (ECA) of pipeline girth welds[C] // The Collected Papers of Pipeline Structure Integrity Technology Workshop, China, Langfang, 2009: 10—11.

[3] Yoo Jangyong. X70 the advantages of the acicular ferrite pipeline steel and the development of the oil and gas industry under adverse circumstances[C] // Academic Report Conferece of Pipeline Steel, China, Langfang, 2003: 18—37.

作者简介: 李建军, 男, 1953年出生, 博士研究生, 高级工程师. 主要从事石油天然气长输管道焊接培训及研究、西气东输等国家重点管道工程的焊接工艺研究. 发表论文 30余篇.

Email: hanjiezhongxin@163.com

[上接第 92页]

[4] 张文钺. 焊接冶金学(基本原理)[M]. 北京: 机械工业出版社, 2005.

[5] 王香云, 王文先, 李结木, 等. BHW35钢焊接接头高温冲击试验分析[J]. 焊接学报. 2010, 31(1): 80—84.
Wang Xiangyun, Wang Wenxian, Li Jiemu, et al. Experimental investigation on impact toughness in high-temperature of BHW35 steel welded joint[J]. Transactions of the China Welding Institution, 2010, 31(1): 80—84.

[6] 赵钦新, 顾海澄, 陆燕荪. BHW35钢中温韧性行为的研究[J]. 动力工程, 1997, 17(2): 64—68, 63.
Zhao Qinxin, Gu Haicheng, Lu Yansun. A study of the toughness properties of BHW35 steel at medium temperature[J]. Power Engineering, 1997, 17(2): 64—68, 63.

作者简介: 王香云, 女, 1962年出生, 硕士, 教授级高级工程师. 主要从事锅炉及压力容器产品及焊接工艺设计研究和材料连接及界面行为. 发表论文 10余篇.

Email: wxyun191@163.com

of Mechanical and Electrical Engineering Kunming University of Science and Technology Kunming 650093 China 2 College of Mechanical Engineering and Applied Electronics Beijing University of Technology Beijing 100124 China). p77—80

Abstract Two level loadings of unequal stress amplitude and unequal mean stress were applied on the two-spot tension-shear spot welds Experimental results show that there exists stress sequence effect under two-level loading There exists exercise effect under low-high loading the damage accumulated by linear damage accumulation rule is higher than 1; there exists overload retardation under high-low loading the damage accumulated by linear damage accumulation rule is also over 1. Under high-low loading residual lives under low stress level are longer than residual life calculated from linear damage accumulation rule some residual fatigue lives are even longer than total life under low stress alone The damage accumulation result under high-low loading indicates that the periphery of spot welds behaves as a notch

Key words: spot weld two level loading damage accumulation notch effect

Effects of forming process of combustion welding rod on manual SHS welding LI Zhizun XIN Wentong HU Renxi HAN Fengqi (Department of Basic Course Ordnance Engineering College Shijiazhuang 050003 China). p81—84

Abstract The influence of forming process of the combustion rod on manual self-propagating high-temperature synthesis (SHS) welding was investigated systematically and the optimum parameters were obtained Results showed that the particle size the forming density and the mixing time had significant effects on the combustion reaction and the welding quality As the particle size of the powder increased welding spatter became severe and a lot of stomata generated in the seam As the particle size decreased the combustion velocity increased and the rod was difficult to operate The optimum particle size to make combustion rod was −260 to +300 mesh It was showed that there was a peak in the forming density and combustion velocity curve The optimum forming density was between 2.74 and 3.05 g/cm³. Results also showed that when the mixing time increased the reaction and spatter became violent But if the mixing time was too short the powder could not contact adequately and the heat generated was not enough to melt the metal The optimum mixing time was 30 min It was showed that the diameter of the rod had not obvious effect on the combustion and it could be determined by the thickness of the weldment

Key words: manual self-propagating high-temperature synthesis welding combustion welding rod forming technology

Effect of process parameters on strengthening of steel surface with Fe-Al intermetallic compounds ZHANG Deku WANG Kehong ZHANG Jing ZHAO Nan (School of Materials Science and Engineering Nanjing University of Science and Technology Nanjing 210094 China). p85—88

Abstract The intermetallic compound $Fe_3Al$ was prepared by plasma arc surface remelting in which the mixture of Al powder and Fe powder was coated on the surface of Q235 steel The effect of plasma arc surfacing parameters on form of coating was studied and appropriate process parameters were obtained The microstructures and the measured Vickers hardness of the coating were analyzed The results indicate that the variation of process parameters such as current swing frequency of welding torch and travel speed closely relates with heat input which has influence on microstructure melting state of substrate interface bonding of substrate and coating and thus the corrosion and wear resistance of the coating is improved greatly The optimum surfacing parameters are a current of 130 A a travel speed of 5 cm/min a swing amplitude of 4 mm and a frequency of 0.4 Hz under this experiment condition

Key words: plasma arc surfacing intermetallic compounds microhardness

Metallograph and high-temperature impact toughness of circumferential joint by SAW of BHW35 steel WANG Xiangyun[1,2] WANG Wenxian HAO Ruihua (1. Taiyuan Boiler Group Co., Ltd., Taiyuan 030021 China 2 College of Materials Science and Engineering Taiyuan University of Technology Taiyuan 030024 China). p89—92 96

Abstract BHW35 steel was welded by automatic submerged-arc welding (SAW) with H08Mn2MoA welding wires and flux HJ350 After stress relief annealing by the postweld heat treatment system impact tests on welded joint and base metal were carried out at 20 100 200 and 350 ℃, and the scanning electron microscopy (SEM) fractograph metallograph hardness and chemical compositions of welding seam were analyzed The results indicate that the highest hardness of HAZ is 291.6 HV The toughness increases greatly compared with that at room temperature The temperature peak value of impact absorbing energy of welding seam occurs at weld of 100 ℃ and both HAZ and base metal of 200 ℃. The impact toughness in HAZ is better than that in welding seam The impact absorbing energy of welded joint is over 47.33 J at room temperature and 134.67 J at 350 ℃, which meets the toughness demand for the welded joint and base metal SEM fractograph indicates that all impact fractures of base metal exhibit ductile dimple and the impact fractures in welded joint at room temperature exhibit quasi-cleavage and ductile dimple With the temperature increasing the fractures subjected high temperature impact all exhibit ductile dimple the better toughness is the more obvious tearing feature of ductile dimple is and the larger the ductile dimple is the more obvious non-uniform distribution is

Key words: BHW35 steel submerged-arc weld joint metallograph and hardness impact absorbing energy fractograph

Welded joint properties of X60 pipeline steel at −20 ℃ LI Jianjun[1,2] DU Zeyu LIU Guangyun LÜ Xiangyang (1. Material School Tianjin University Tianjin 300072 China 2 China Petroleum Pipeline Welding Training Center Langfang 065000 China). p93—96

Abstract In accordance with the site construction of X60 pipeline steel at −20 ℃, the mechanical properties metallograpic structure hardness Charpy impact absorbing energy and the fracture structure of the girth welded joints of $\phi 711 \times 15.9$ mm pipeline are analyzed The results show that the highest HAZ hardness value of the X60 pipe steel joints girth-welding

at −20 ℃ cryo-welding is 210 HV10 which meets related standards. The welding procedure specification has been used on the long-distance pipeline projects in China's northern area, which obtains satisfactory results: no hardened structures in the joints through metallurgical microscopic observation and the toughness of the joints meeting the requirement of related technical standards through microscopic observation of the cross section of the Charpy test sample.

Key words: X60 pipeline steel; −20 ℃ cryo welding; welded joint properties

Application of ultrasonic sensor to broken line tracking of corrugated board TIAN Songya, SHI Rusen, ZHU Xiaohua, YANG Quanhai, CHEN Lihua (1. College of Electromechanical Engineering, Hohai University, Changzhou 213022, China; 2. Zhangzhou Institute of Mechatronic Technology, Changzhou 213164, China). p 97−100

Abstract: Ultrasonic sensor produced by Banner was used to track a period of broken line for corrugated board at three velocities, and TMS320LF2407A was used to sample the analog signal of the sensor and transform it to digital signal. Through the function of fast Fourier transform, the sample data was analyzed to get the frequency range of target signal. Then a Butterworth digital filter was designed. Filtered data showed that the waveforms at the three velocities were very similar, the signal changed significantly at the junction position between groove and hypotenuse surface of the corrugated board, and the signal were leading or lag at the junction position between the top and hypotenuse surface of the corrugated board because of the characteristics of the scattering and reflection of ultrasound. The former was chosen target position. The broken line from the given point was tracked repeatedly at welding tractor speed of 500 cts/s. The results indicated that the signal mutational site was the broken position, and the error range was −0.60 to −0.04 mm.

Key words: ultrasonic sensor; broken line tracking; fast Fourier transform; digital filtering

TiC particle reinforced Fe-based composite coatings processed by submerged-arc welding adding of alloy powder LIU Junhai, HUANG Jihua, LIU Junbo, SONG Guixiang (1. School of Materials Science and Engineering, University of Science and Technology Beijing, Beijing 100083, China; 2. Department of Mechanical and Electronic Engineering, Weihai Vocational College, Weihai 264210, China; 3. Department of Mechanical and Electronic Engineering, Weifang University, Weifang 261041, China; 4. Department of Vocational Skills Training Center, Weihai Vocational College, Weihai 264210, China). p 101−104

Abstract: TiC particle reinforced Fe-based composites coatings were in situ synthesized on surface of Q235 steel by submerged arc welding of the compacts of mixed ferrotitanium, ferrochromium, iron and carbon powers, etc. The coating was without cracks, inclusions, porosity and other defects, no need to preheat before welding and slow cooling after welding. Microstructures of the coating were observed by scanning electron microscope (SEM), X-ray diffraction (XRD) and Energy Disperse Spectroscopy (EDS), and microhardness was measured by microhardness tester. The results indicated that the fine TiC particles were formed by using submerged arc welding process and distributed in the matrix, and the particles sizes were under 2 μm. The microstructure of the coating consisted of TiC particles, martensite and austenite, and the microhardness of the coating was up to 601 HV0.2, which was about 3 times of that of the based metal.

Key words: submerged arc welding; TiC particle; coating; in situ formation

Analysis of T-joint weld shaping characteristics and influencing factors by laser-TIG hybrid welding titanium alloy WANG Miao, GU Kanfeng, WEI Qiang, YU Ying, WU Lin, CHEN Yanbin (1. State Key Laboratory of Advanced Welding Production Technology, Harbin Institute of Technology, Harbin 150001, China; 2. Shenyang Institute of Automation, Chinese Academy of Sciences, Shenyang 110016, China; 3. Shenyang University of Aeronautics and Astronautics, Shenyang 110136, China). p 105−108

Abstract: A new laser-TIG (laser beam and tungsten inert gas) hybrid welding procedure for titanium alloy T-joint structure called single pass welding and double backside shaping technology is proposed. The forming properties of the T-joint structure is analyzed and discussed under different testing conditions by a series comparative welding experiments to reveal the optimal scheme of single pass welding and double backside shaping with laser-TIG hybrid welding for titanium alloy T-joint structure. The results indicate that comparing with the TIG melt through welding methods, the proposed single pass welding and double backside shaping technology based on laser-TIG hybrid welding procedure for titanium alloy T-joint structure is obviously advantageous in weld forming, weld microstructure, weld composition, weld property, welding efficiency and the tolerance to gaps between plates.

Key words: titanium alloy; T-joint; hybrid welding; weld forming

Experimental analysis of explosive welding of NiTi alloy DING Yanjun, TONG Zheng, LI Jinfu, LIN Yulong (1. College of Materials Science and Engineering, Inner Mongolia University of Technology, Hohhot 010051, China; 2. Explosion Processing Mill, Beijing Haoyu Industry and Trade Co. Ltd., Beijing 102300, China). p 109−112

Abstract: The explosive welding technology for unannealed NiTi shape memory alloy is studied by means of the lower limit method and the design of structure of rigid buffering layer. The chemical composition and structure of welding materials are analyzed with optical microscopy, scanning electron microscope and energy disperse spectroscopy. The results show that the explosive welding of unannealed NiTi shape memory alloy is possible by replacing the flexible buffering layer with the rigid buffering layer and using rigid anvil. The explosive welding has little effect on the chemical composition of welding materials, only a few grain refinement in transition region which is 100 μm from the weld joint. The chemical compositions of the weld joint and the base material are basic identical. It has an important significance that keeps the shape memory function of the NiTi alloy.

Key words: NiTi shape memory alloy; explosive welding; lower limit method; microstructure